

A tunable microwave circulator based on a magnetized plasma as an active gyrotropic element

Cite as: Phys. Plasmas **29**, 112114 (2022); <https://doi.org/10.1063/5.0123459>

Submitted: 30 August 2022 • Accepted: 23 October 2022 • Published Online: 11 November 2022

 Hossein Mehrpour Bernety,  Luc S. Houriez,  Jesse A. Rodríguez, et al.



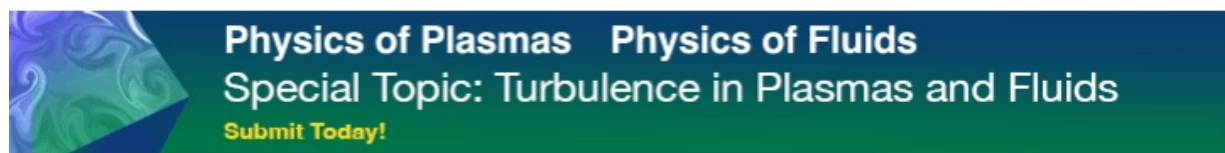
[View Online](#)



[Export Citation](#)



[CrossMark](#)



Physics of Plasmas Physics of Fluids
Special Topic: Turbulence in Plasmas and Fluids
Submit Today!

A tunable microwave circulator based on a magnetized plasma as an active gyrotropic element

Cite as: Phys. Plasmas **29**, 112114 (2022); doi: [10.1063/5.0123459](https://doi.org/10.1063/5.0123459)

Submitted: 30 August 2022 · Accepted: 23 October 2022 ·

Published Online: 11 November 2022



View Online



Export Citation



CrossMark

Hossein Mehrpour Bernety,^{a)}  Luc S. Houriez,  Jesse A. Rodríguez,  Benjamin Wang, 
and Mark A. Cappelli 

AFFILIATIONS

Department of Mechanical Engineering, Stanford University, Stanford, California 94305, USA

^{a)} Author to whom correspondence should be addressed: bernety@stanford.edu

ABSTRACT

We present a theoretical analysis and experimental demonstration of a microwave circulator that uses a magnetized plasma as the gyrotropic element. Unlike traditional circulators that exploit the anisotropic permeability of ferrite, here, we exploit the anisotropic dielectric constant of a magnetized plasma to achieve non-reciprocity. The advantage of a plasma-loaded circulator is that it allows for tunability, and modulation that is limited in speed by the ionization/recombination time of the plasma. The theoretical analysis treats the problem of electromagnetic scattering from a heterogeneous gyrotropic plasma rod to confirm scattering behavior and to guide in defining the design parameter space covered by more detailed computational simulations. Proof-of-concept experiments are carried out using a custom-fabricated low-frequency gas discharge tube as the plasma element. Here, we confirm the plasma-frequency dependent tunability predicted by the simulations, demonstrating this tunability in the experiments by varying the applied discharge voltage. These initial experiments suggest that isolation in excess of 25 dB is achievable, in reasonable agreement with the theory and simulations for studies in the S and C ranges of the microwave spectrum.

Published under an exclusive license by AIP Publishing. <https://doi.org/10.1063/5.0123459>

I. INTRODUCTION

A circulator is a non-reciprocal device that most commonly consists of three ports and provides power flow between ports in a clockwise or counter-clockwise fashion.¹ An ideal circulator would have zero reflection at all ports, zero insertion loss in the forward direction (i.e., from one port to its intended receiving port), and infinite isolation in the reverse direction (i.e., from one port to the intended isolated port).² A circulator can be used as an isolator by connecting a matched load to one of the ports. Microwave circulators in this configuration are widely used to isolate a receiver from a transmitter acting as a duplexer,^{3,4} and also, in space and ground communication systems.^{5,6}

Circulators can be categorized as belonging to the ferrite⁷ or non-ferrite class. The most common are the passively magnetically biased ferrite based designs. Of these, there are various types, such as those based on the use of striplines,^{8–11} microstrips,^{2,3,12} empty substrate integrated coaxial lines,¹³ ridge gap waveguides,¹⁴ spoof surface plasmons,¹⁵ ferromagnetic nanowires,¹⁶ mechanical on-chip devices,¹⁷ and photonic crystals.¹⁸

In recent years, non-ferrite circulators have also caught the interest of researchers and engineers. Early studies of this type have been

more focused on active circulators that use transistors as the switching elements.^{19,20} Such designs have power and noise limitations as addressed in the literature.²¹ For use at higher power, junction circulators and phase shifters are preferred.¹⁴ It has been proposed that graphene can be a good candidate to realize circulators at terahertz (THz) frequencies.²² It is noteworthy that symmetry-breaking non-reciprocity can also be achieved by other methods,²³ such as by exploiting non-linearities²⁴ or by time modulation.^{25,26} Possible techniques have been covered in detail by Kord *et al.*²³

The more common ferrite-based circulators break symmetry through the application of a magnetic bias to the ferrite to generate an anisotropic permeability tensor. In general, these are not tunable when biased by a permanent magnet, and although electromagnets do afford some degree of tunability, the rate is limited by the inductance of the circuit. We examine here, in this paper, the use of a magnetized plasma as an alternative to ferrite. A magnetized plasma that can be tuned or modulated at higher rates by varying plasma density limited mainly by time scales associated with ionization and recombination.

A magnetized plasma has an anisotropic permittivity²⁷ that, like biased ferrite, results in a gyrotropic response. This property also leads

to non-reciprocity. In addition to their use as a substitute for ferrite in circulators, a magnetized plasma element may enable the development of tunable/reconfigurable one-way waveguides and other types of isolators. Systems that employ plasmas enable the preferred use of permanent magnets (which can achieve much higher bias), while by varying plasma density to achieve tunability.²⁸

This paper is structured as follows. In Sec. II, we present the analytical theory that guides the circulator design using commercial software and then details of the construction of the device. The theory is based on the analysis of the electromagnetic (EM) scattering from a magnetized, weakly collisional plasma rod, the axis of which is aligned with the external magnetic bias. The plasma is modeled to be heterogeneous in its construction, accounting for the quartz envelope and low-density region in the envelope’s vicinity. Once the required conditions for such a circulator are found, a three-dimensional (3D) simulation is carried to guide the design and fabrication of the prototype to be tested. In Sec. III, we describe the experiments carried out in a facility that enables varying the relatively uniform magnetic bias that is applied with electromagnets as well as varying the operating potential applied to the discharge plasmas that are integrated into the device structure. A brief discussion and summary are offered in Sec. IV.

II. ANALYTICAL ANALYSIS AND SIMULATIONS

We consider a uniform transverse electric (TE^z) plane wave traveling along *x*-axis and normally incident upon the rod in a plane perpendicular to the rod axis (i.e., *z*-axis), as shown in Fig. 1. The rod consists of a quartz wall and a cylindrical plasma column, separated by an un-ionized layer.

The incident magnetic field, \mathbf{H}^i , can be expressed as an infinite sum of cylindrical wave functions,

$$\mathbf{H}^i = \hat{\mathbf{z}}H_z^i = \hat{\mathbf{z}} \sum_{n=-\infty}^{\infty} j^{-n} J_n(k_0 \rho) e^{jn\varphi}, \quad (1)$$

with k_0 representing the free space wave number and J_n is the Bessel function of the first kind. The scattered magnetic field can be expressed as

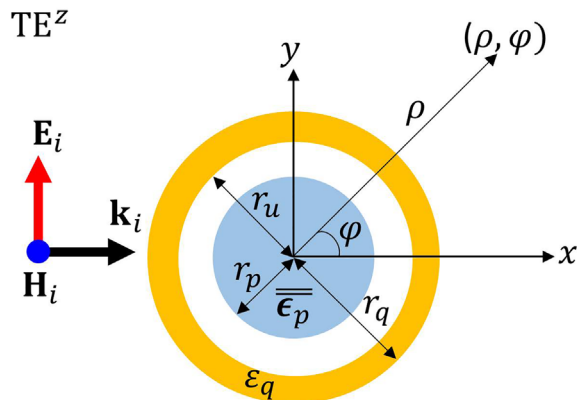


FIG. 1. Schematic of the three-layer cylindrical model of a plasma discharge rod under normal TE plane wave incidence. An external applied magnetic bias is aligned along the *z*-direction.

$$\mathbf{H}^s = \hat{\mathbf{z}}H_z^s = \hat{\mathbf{z}} \sum_{n=-\infty}^{\infty} a_n H_n^{(2)}(k_0 \rho) e^{jn\varphi}. \quad (2)$$

The magnetic field inside the quartz shell (\mathbf{H}^q), with relative permittivity of ϵ_q is

$$\mathbf{H}^q = \hat{\mathbf{z}} \sum_{n=-\infty}^{\infty} [b_n J_n(k_q \rho) + c_n Y_n(k_q \rho)] e^{jn\varphi}. \quad (3)$$

The magnetic field inside the un-ionized layer (\mathbf{H}^u) is

$$\mathbf{H}^u = \hat{\mathbf{z}} \sum_{n=-\infty}^{\infty} [B_n J_n(k_0 \rho) + C_n Y_n(k_0 \rho)] e^{jn\varphi}. \quad (4)$$

Using Ampère’s law, one can determine the corresponding electric fields in the quartz and un-ionized gas layer. Finally, both the magnetic and electric fields inside the magnetized plasma (\mathbf{H}^p and \mathbf{E}^p), the relative permittivity of which is $\bar{\epsilon}_p$, can be expressed as

$$\mathbf{H}^p = \hat{\mathbf{z}}H_z^p = \hat{\mathbf{z}} \sum_{n=-\infty}^{\infty} d_n J_n(k_p \rho) e^{jn\varphi}, \quad (5)$$

$$\mathbf{E}^p = \frac{1}{j\omega\epsilon_0} \bar{\epsilon}_p^{-1} \cdot (\nabla \times \mathbf{H}^p) = E_\rho^p \hat{\rho} + E_\varphi^p \hat{\varphi}. \quad (6)$$

For a plasma rod that is biased with a magnetic field aligned along the *z*-direction, the relative permittivity (dielectric constant) of the plasma is given as

$$\bar{\epsilon}_p = \begin{bmatrix} \epsilon_t & j\epsilon_g & 0 \\ -j\epsilon_g & \epsilon_t & 0 \\ 0 & 0 & \epsilon_z \end{bmatrix} \quad (7a)$$

and

$$\epsilon_t = 1 - \frac{\omega_p^2(\omega - j\nu_c)}{\omega[(\omega - j\nu_c)^2 - \omega_b^2]}, \quad (7b)$$

$$\epsilon_g = -\frac{\omega_p^2 \omega_b}{\omega[(\omega - j\nu_c)^2 - \omega_b^2]}. \quad (7c)$$

Here, ω_p , ω_b , and ω are the plasma, electron cyclotron, and field frequencies, respectively, and the wave damping due to electron scattering with the background gas is denoted by ν_c . We assume that frequencies are sufficiently high that the effect of ion motion is negligible. For the EM scattering, the boundary conditions are that the tangential components of the electric and magnetic fields are continuous at the boundaries. The resulting matrix equation is solved to find the unknown coefficients in the above field expansions.

A. Connecting the scattering problem to the circulator design

A circulator is generally a three-port device. Within such a device, an incoming signal from a port, say, port 1, will be directed to port 2, and similarly, from port 2 to port 3, and from port 3 to port 1, say, in a clock-wise fashion, in the device illustrated schematically in Fig. 2. In this figure, the applied magnetic bias is assumed to be along *z*-axis. In contrast to that of a ferrite-based circulator, the electric field

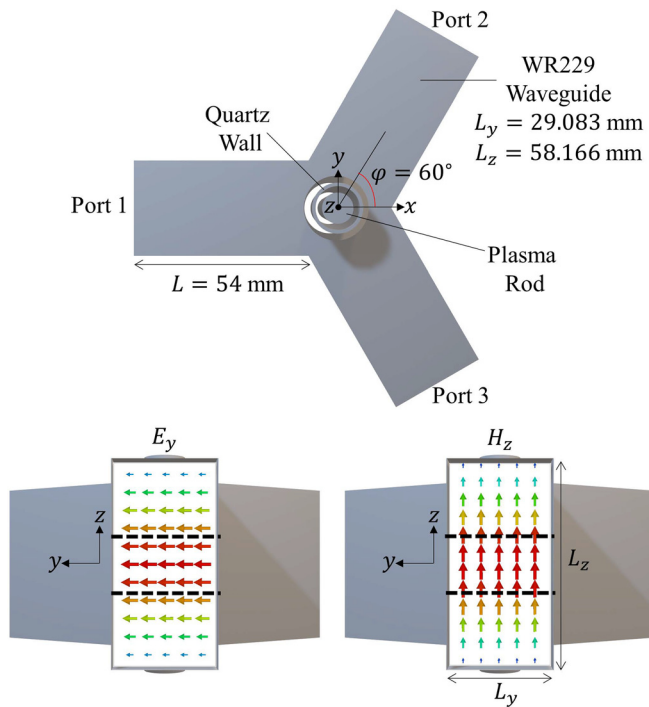


FIG. 2. Schematic illustration of the circulator design (top) and the field distributions at the aperture of an input ports (bottom left, E_y , and right, H_z).

must be oriented along a perpendicular to the applied bias, which, in this configuration shown, is aligned with the axis of the rod, to achieve the required non-reciprocity. In the figure, and in the subsequent analysis and experiments, we define dimensions for a device constructed out of three WR229 waveguides, with the biased plasma located at the intersection between them. These waveguides are typically used for transmission of EM waves over the frequency range of 3.3–4.9 GHz, with a lower cutoff of about 2.6 GHz and an upper cutoff at approximately 5.2 GHz, i.e., straddling the S and C bands.

To connect the scattering problem to the design of a practical circulator, we begin by examining the electric and magnetic field modes that propagate within a rectangular WR229 waveguide. These are illustrated in the lower, left, and right images shown in Fig. 2. For $-L_y/2 < y < L_y/2$ and $-L_z/2 < z < L_z/2$, the fields of the dominant mode (the TE₁₀ mode), traveling along x -axis, at the aperture of the input port (i.e., port 1) are²⁹

$$E_y = E_{0,y} \sin\left(\frac{\pi}{L_z}\left(z - \frac{L_z}{2}\right)\right), \tag{8a}$$

$$H_z = H_{0,z} \sin\left(\frac{\pi}{L_z}\left(z - \frac{L_z}{2}\right)\right), \tag{8b}$$

$$H_x = H_{0,x} \cos\left(\frac{\pi}{L_z}\left(z - \frac{L_z}{2}\right)\right), \tag{8c}$$

where $E_{0,y}$, $H_{0,z}$, and $H_{0,x}$ are constants, and L_z is the largest of the dimension of the waveguide cross section shown in the lower images of Fig. 2.

It is apparent that the magnitude of the E_y and H_z components is maximum at $z=0$, but the magnitude of the H_x component is minimum at $z=0$ and maximum at $z = \pm L_z/2$. The main task of the circulator is to redirect fields from port 1 to port 2, from port 2 to port 3, and from port 3 to port 1 on the $z=0$ plane. As a result, the H_x component will not affect the performance of the circulator, and the E_y and H_z components are the ones involved in its operation (shown in Fig. 2). In other words, one can consider the incoming wave around $z=0$ as a window of a transverse electric (TE^z), uniform plane wave as highlighted using dashed lines in Fig. 2. Such a consideration allows us to design a circulator by investigating the electromagnetic scattering of a free-space, normally incident plane wave from a gyrotropic plasma rod. With this analysis, we can gather insight as to the required conditions that will guide the design and operating conditions a plasma-based circulator for efficient isolation over a specified range of microwave frequencies.

B. Free-space scattering and circulator design

The plasma rod used in our analysis (see Fig. 1) and subsequent experiments is a custom-fabricated fluorescent ultraviolet (UV) discharge tube with a uniform plasma radius taken to be $r_p = 4.6$ mm, an inner quartz envelope radius to be $r_a = 6.5$ mm, and an outer quartz envelope to be $r_q = 7.5$ mm. These discharges and their estimated plasma properties have been described in several of our prior studies,^{26,28,30–32} which have used them in the construction of various plasma photonic crystals. The un-ionized space (of unity dielectric constant) between the plasma and inner boundary of the quartz tube is modeled to account for the low density region within the sheath and pre-sheath (ambipolar diffusion layer), which exists at the quartz-plasma boundary. In these earlier studies, plasma properties were derived from measured root mean square (RMS) current and peak-to-peak voltages and an estimated current-carrying cross sectional area that provides a radially averaged plasma density equivalent to that assuming a parabolic radial profile, which approximates that which would be generated from uniform ionization balanced by diffusion. Transport coefficients needed for the analysis were determined using the BoltSig+ electron energy distribution function solver.³³ We understand that this is only an approximate approach to determining the plasma discharge properties, and it is recognized that in our previous studies, the plasmas were not magnetized. Here, we may expect that the plasma radius may be somewhat smaller because of the magnetic bias and associated plasma confinement. In a very recent study of ours,³⁴ which mapped out the scattered fields from the same (but magnetized) plasma discharge tube, the use of this plasma cross section did result in slightly higher derived plasma density than that estimated from previous non-magnetized studies, which is expected. The theoretical analysis and simulations are just a first step for the design of the circulator, and fine tuning of the performance is achieved by examining the response over a range of operating frequency, as described in Sec. III. Finally, the relative permittivity of the quartz layer is taken to be $\epsilon_q = 3.75$.

Considering the configuration of the circulator and the parameters of the coordinates shown in Fig. 1, to direct the incoming fields from, say, port 1 to port 2 of Fig. 2, the magnetized plasma rod should rotate the Poynting vector of scattered fields by $\phi = 60^\circ$. Although one needs only to examine the near fields to achieve this scattering objective, to narrow down the search, we may start with an analysis of

far fields, i.e., the scattering width of the rod impinged by a normal plane wave with TE^z polarization. We assume that our design frequency is in the vicinity of $f = 4$ GHz, and a value for the electron collisional damping frequency, $\nu_c = 1$ GHz, and a plasma frequency, $f_p = \omega_p/2\pi = 7$ GHz. These conditions for the plasma are close to that extracted from the recent near-field scattering measurements mentioned above.³⁴ In Fig. 3, we compute the bistatic scattering normalized to the wavelength, i.e., σ_{2D}/λ , for different values of cyclotron frequency, $f_b = \omega_b/2\pi$, which is linearly dependent on the magnetic bias field, B_0 , i.e., $f_b = eB_0/(2\pi m_e)$. Here, m_e and e are the electron mass and charge, respectively. In the figure, the solid lines represent that determined by the analytical model. For comparison, we have also computed the bistatic scattering using CST Microwave Studio and represent these as the dashed lines. It is apparent that the analytical model produces the same bistatic scattering as that computed using CST. This confirms that the simple model can be used to identify conditions for a desired scattering angle. We also see that by increasing B_0 , or as a result, the cyclotron frequency (f_b), the angle defining the maximum in the bistatic scattering, increases. In designing a circulator, one desires that the angle between waveguide ports coincides with the maximum scattering computed for the frequency range of interest, and the range of plasma conditions accessible. Here, as we are interested in waveguide circulators that have ports separated by 120°, we desire $\varphi = 60^\circ$ —scattering that can be achieved with $f_b = 1.85$ GHz, $f_p = 7$ GHz, and $\nu_c = 1$ GHz, and for the operation frequency of $f = 4$ GHz used here. Since the bistatic scattering is a far-field concept, a more refined design targeting specific frequencies of operation given plasma parameters requires computing near-field scattering power. Figure 4 plots the CST-simulated normalized near-field scattered power [in dB, i.e., $(10 \log_{10}[|H_z^s|^2/|H_z^s|_{\max}^2])$], for the above plasma conditions. We find that the near-field scattering is also preferably in the vicinity of $\varphi = 60^\circ$. With the identified plasma conditions and geometry, we can examine the isolation capability of the magnetized plasma rod when used in the circulator design shown in Fig. 2.

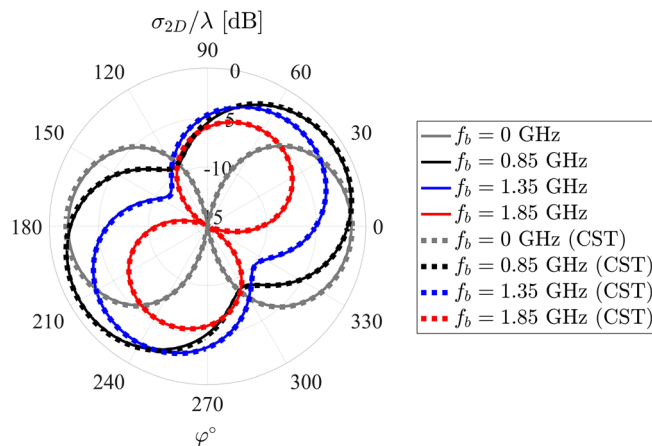


FIG. 3. Bistatic scattering width (in dB) of the modeled magnetized plasma column of Fig. 1, for different values of cyclotron frequency, f_b (in GHz), corresponding to the magnetic field intensities of $B_0 = 0, 30.4, 48.3,$ and 66 mT. The solid lines are the results of the analytical calculation, while the dashed lines are that computed using CST.

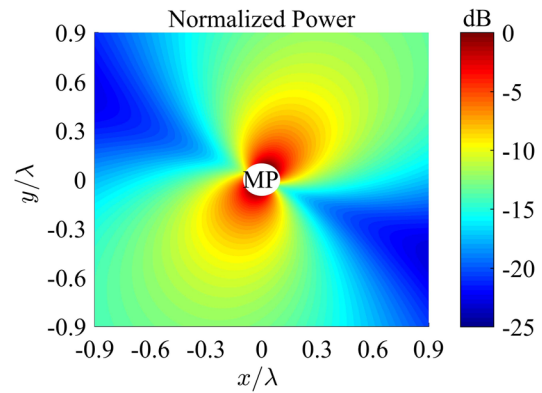


FIG. 4. Normalized scattered power from the model magnetized plasma column in the near-field region. Plasma, cyclotron, and field frequencies are $f_p = 7, f_b = 1.85$ GHz, and $f = 4$ GHz, respectively.

Full CST simulations are carried out of the three-dimensional circulator shown in Fig. 2 to predict the isolation capability when plasma-loaded. The resulting S-parameters are shown in Fig. 5. In these simulations, waves are launched into the device using the “waveguide ports” feature of CST. While we determined from the analytical study above that optimum scattering occurred for a plasma frequency, $f_p = 7$ GHz, we also show the computed S-parameters for $f_p = 6.8$ GHz and 7.2 GHz. Better performance, defined by the isolation, $S_{31} - S_{21}$, is seen at approximately 3.975 GHz, for the $f_p = 6.8$ GHz case. For the intended plasma $f_p = 7$ GHz case, the best isolation seems to occur at $f = 4.1$ GHz, and the values for the return loss, insertion loss, and isolation are 1.2, 14, and 22 dB, respectively. A color map of the normalized power, in dB ($10 \log_{10}[|H|^2/|H|_{\max}^2]$) at a snapshot in time, delivered from port 1 to port 2 is shown in Fig. 6. We find that the magnetized plasma column efficiently redirects the power to port 2, while minimizing the power delivered to port 3, confirming the effectiveness of the design. It is noteworthy that a close inspection of the fields depicted in Fig. 6 reveals that the EM waves penetrate the plasma despite that the field frequency (4.1 GHz) is well below that of the cutoff of the lower extraordinary (X) mode of the

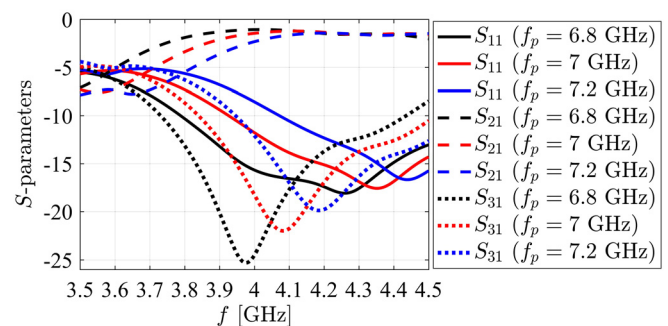


FIG. 5. CST-computed S-parameters for the circulator design of Fig. 2 with a magnetic bias corresponding to $f_b = 1.85$ GHz, and various plasma frequencies corresponding to the plasma densities of $n_0 = 5.75 \times 10^{11}, 6.1 \times 10^{11},$ and $6.45 \times 10^{11} \text{ cm}^{-3}$.

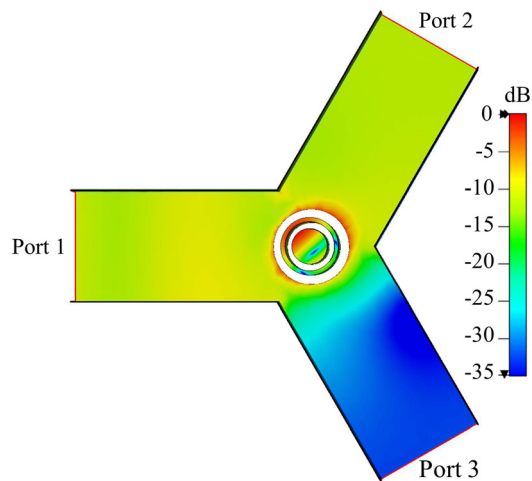


FIG. 6. Computed normalized power flowing into ports 2 and 3 with port 1 excited, for the $f_p = 7$ GHz and $f = 4.1$ GHz case of Fig. 5.

magnetized plasma,²⁷ $f_1 = \sqrt{f_p^2 - f_b^2}/4 - f_b^2/2$. For these conditions, this cutoff $f_1 = 4$ GHz, approximately that of the electron cyclotron frequency and considerably less than the modeled plasma frequency $f_p = 7$ GHz. Transmission of the plasma is a consequence of tunneling of the EM fields,³⁵ as the skin for the X-mode³⁶ is of the same scale as that of the plasma diameter.

III. EXPERIMENTAL DEMONSTRATION

A device is built leveraging the understanding gathered from the above theory and simulations, to experimentally confirm the plasma's gyrotropic response and to assess the circulator performance. These studies provide initial data that may guide further plasma-loaded circulator performance improvements. While the experiments described below span the S and C bands of the microwave spectrum, in principal, provided that plasmas of higher or lower densities can be generated, designs can be appropriately scaled for performance at higher or lower frequency bands.

A. Circulator fabrication

As shown in Fig. 7, a 3D virtual model of the circulator was constructed using the Computer Aided Design (CAD) software called Fusion 360. The model's geometry was guided by the CST simulations shown in Fig. 2. A center bore is included to allow for the plasma rod to be inserted, and each port supports a flange for an SMA (SubMiniature version A) to waveguide adapter. The CAD model is 3D printed using a resin printer. Figure 8 shows the 3D printed part as it is being cured under natural sunlight. The print is then sanded and copper electroplated. The copper layer thickness is estimated to be 0.1 mm, which is approximately 100 times the copper's skin depth at the GHz scale, making the electroplated print an effective waveguiding material in this S–C band microwave regime.

An HP 8722D Vector Network Analyzer (VNA) was connected via SMA cables to the circulator's waveguide adapters to probe the response of the device. The HP 8722D is a two-port VNA. As such, S-Parameter measurements are taken in two steps. First, S_{21} is measured

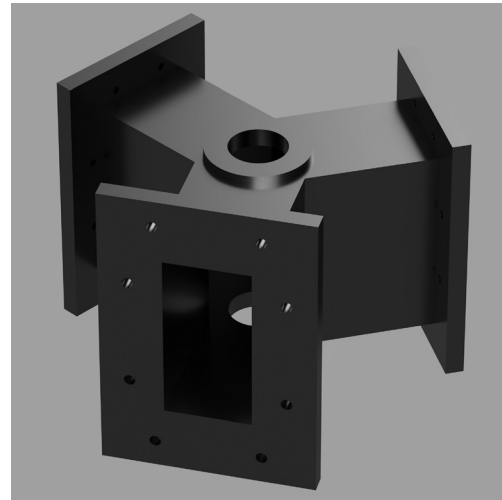


FIG. 7. Plasma circulator 3D model designed and rendered using the CAD software called Fusion 360.

by connecting port 2 and port 1 to the VNA. Second, S_{31} is measured by disconnecting port 2 and connecting port 3. We note, however, that as we are using a two-port VNA on a 3-port device, these measurements do not generate true three port S-parameters, and without the knowledge of the reflection coefficient of the open port, we do not attempt to determine the true S-parameters. The S-parameters presented here, nevertheless, afford a means of evaluating the isolation capability of the magnetized plasma and comparing this isolation to cases where the plasma is turned off. Prior to data collection, a full 2 port calibration of the system is carried out using an Agilent Calibration Kit.

For the S-parameter measurements, the plasma rod is inserted in the center bore, and the entire device is positioned within Helmholtz coils for axial magnetization of the column. The coils, powered in

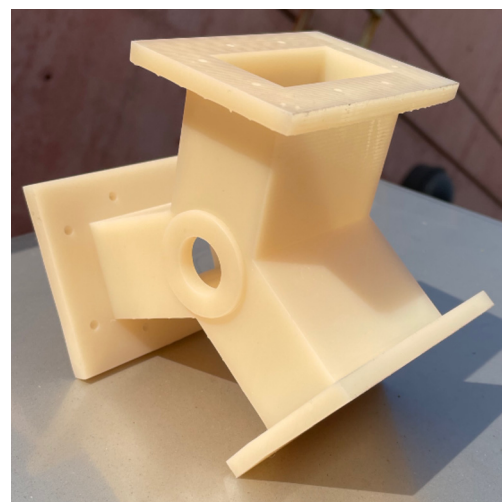


FIG. 8. Plasma circulator resin print undergoing curing in natural light.

series by a 10 A, 100 V power supply, provide a quasi-uniform magnetic field, which can reach as high as 47 mT. The coil spools are conduction cooled by circulating water at 2.5 °C to 8 aluminum pods in contact with the spool’s surface to compensate for the resistive heating within the coil winding. Figure 9 provides a photograph of the experimental setup with the plasma ignited and magnetized. In this photograph, we see the completed copper-plated circulator body.

The plasma discharge, partly described in Sec. II, is 290 mm in length and filled with approximately 250 Pa of argon and added mercury, the vapor pressure of which is determined by the operating temperature. The gas temperature during nominal operation is approximately 330 K, resulting in a mercury vapor partial pressure of about 3.5 Pa. The discharge is driven by an alternating-current (AC) ballast. The plasma density is tuned by using a variable AC transformer (Variac) to adjust the AC (root mean square—RMS) voltage delivered to the ballast. For the results presented below, the Variac RMS output voltages were 50, 60, 80, and 100 V, corresponding to ballast output peak-to-peak (pp) voltages (RMS discharge currents, average power) of 172 V (117 mA, 6.4 W), 160 V (149 mA, 7.5 W), 144 V (234 mA, 9.5 W), and 132 V (307 mA, 10.7 W), respectively. As a reference point, we have estimated from prior scattering studies under comparable magnetic field strengths that for a discharge operating at 144 V pp (but slightly higher current), the plasma frequency, corresponding plasma density, and electron collisional damping were found to be 8.4 GHz, $8.8 \times 10^{11} \text{ cm}^3/\text{s}$, and 1.3 GHz, respectively.³⁴ Figure 10 provides a block diagram of the entire experimental setup.

B. Measurement

Four experimental configurations are investigated to understand the overall scattering response of this plasma-loaded circulator. In the first configuration, the device is free of a plasma rod. The measured S-parameters of this run are presented in Fig. 11(a). We see that the S_{21} and S_{31} are identical, confirming the symmetry of the device, with equal transmission to either port 2 or port 3. We also see, for example, the mode centered at 3.5 GHz has minimal return losses (S_{11}) when the transmission to ports 1 and 2 is high. In the second configuration, the plasma rod is inserted but not ignited. As shown in Fig. 11(b), the

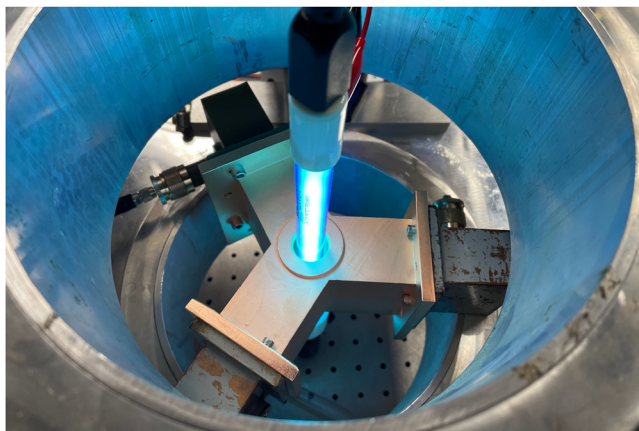


FIG. 9. Laboratory photograph of the experimental setup showing the plasma circulator in the Helmholtz coils as the plasma is ignited and magnetized.

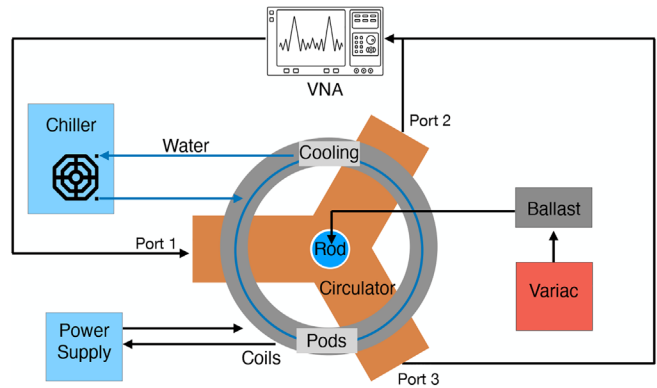


FIG. 10. Block diagram depicting the functional elements of the entire experimental setup.

quartz walls of the plasma rod seem to have very little influence on the measured S-parameters. In the third run, the plasma’s ionization is sustained by providing a 50 V difference to the ballast. The measured S-parameters are presented in Fig. 11(c). In all of these first three configurations, the magnetic coils are not active. We see from Fig. 11(c) that the device still has a symmetric response, but the transmission (and backreflection) resonances have broadened significantly, and the S_{11} appears more rich in its structure, introducing two new low reflection peaks at 3.75 and 4.5 GHz. The ignition of the non-magnetized plasma of plasma frequency above that of the EM radiation will cause some reflection, introducing new waveguide modes. In the fourth configuration, with the plasma ignited as in the case of Fig. 11(c), the magnetic coils are switched on to provide a 47 mT magnetic bias to the plasma, favoring scattering into port 2. The measured S-parameters for this last run are shown in Fig. 11(d). We see that while the S_{11} is relatively unchanged, the attenuation peaks of the S_{31} narrow dramatically, whereas the S_{21} broadens, experiences an overall increase in transmission, and shifts slightly, to higher frequency, by about 1 GHz. The increased signal into port 3 when introducing the magnetic bias rotates the scattering pattern as discussed above, breaking the scattering symmetry. The regions of elevated S_{21} are concomitant with a more strongly attenuated S_{31} .

Examining the measured S-parameters for this 50 V case more closely, we see that in some frequency bands, this isolation, defined by the port transmission difference $S_{21} - S_{31}$, is substantial. Figure 11(d) shows that this configuration achieves a 21 dB isolation between S_{21} and S_{31} in the vicinity of 3.2 GHz. Additionally, S_{11} is lower than S_{21} across almost all probed frequencies demonstrating low return losses. It is noteworthy, however, that the introduction of the plasma (following ignition) does introduce dissipative losses arising from electron scattering collisions. The impact of this damping is apparent in the parameters depicted in Fig. 11(c). We see that the port transmission represented by the measured S_{21} and S_{31} parameters is attenuated by as much as 3.5 dB compared to the non-ignited case of Fig. 11(b). We also see an isolation of 10 dB at 3.75 GHz, and about 7 dB at 4.5 GHz. The attenuation peaks are also significantly broadened. For this plasma condition, we believe the plasma density to be approximately $6 \times 10^{11} \text{ cm}^3/\text{s}$ ($f_p = 7 \text{ GHz}$),³⁷ and, as discussed earlier, the introduced plasma is overdense at these frequencies.

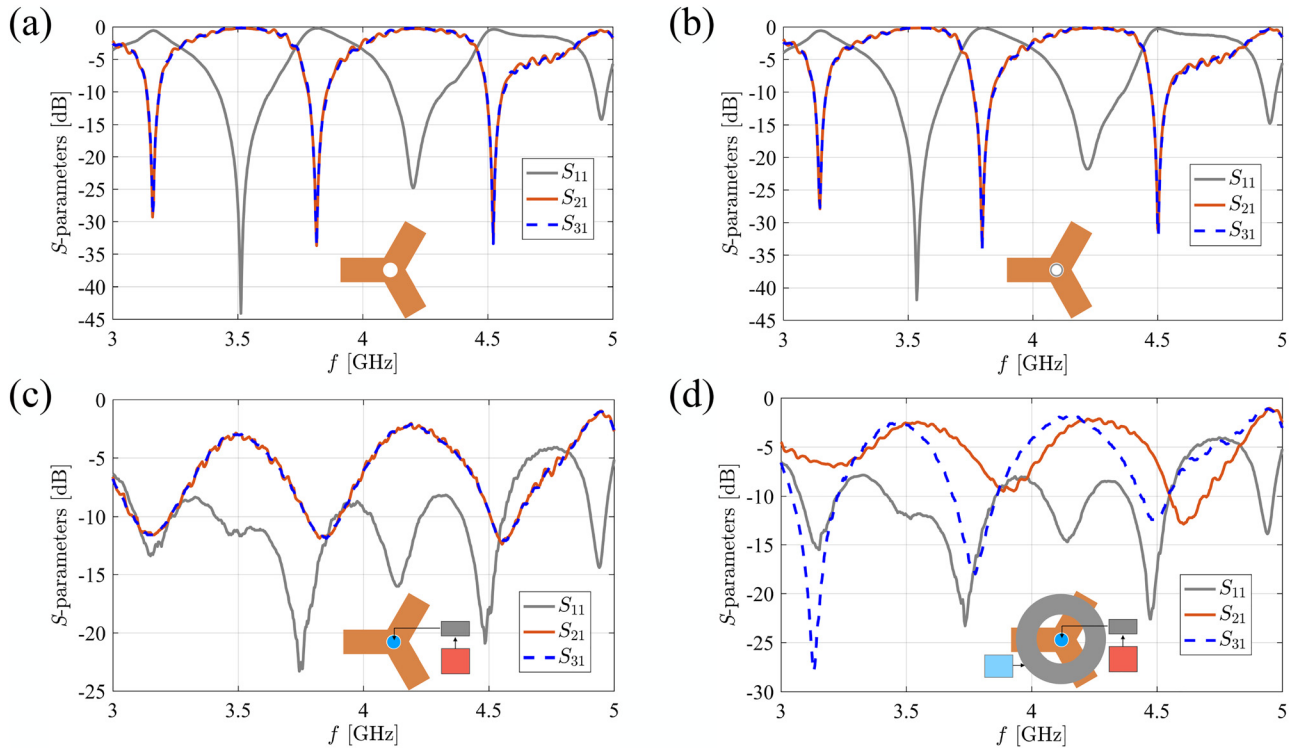


FIG. 11. S-parameters measurements for four different configurations: (a) the device is free of the plasma rod; (b) the plasma rod is inserted but not ignited; (c) the plasma rod is inserted and the plasma's ionization is sustained by supplying a 50 V difference to the ballast; and (d) the plasma's ionization is sustained by applying a 50 V difference to the ballast, while the Helmholtz coils provide a 47 mT magnetic field to magnetize the plasma.

The main benefit of using a plasma rod instead of a ferrite element in a circulator is the ability to easily tune the device by varying the voltage applied to the discharge ballast (here, 50–100 V). This varies the power dissipated in the plasma, and, correspondingly, the plasma density/plasma frequency. An example of this is shown in Fig. 12(a), which, for a fixed cyclotron frequency $\omega_b = 8.3 \times 10^9$ rad/s, plots the strength of the isolation, defined here as $S_{21} - S_{31}$ for these

three voltage cases. The data reveal that lower discharge voltages (lower plasma density) favor isolation at lower frequencies, although the strength of the isolation (nearly 25 dB) is greatest for the 60 V case at 3.2 GHz. In a similar fashion, as shown in Fig. 12(b), we tune the cyclotron frequency by varying the applied voltage to the external Helmholtz coils while maintaining a constant discharge voltage through an applied Variac voltage of 60 V. The variations in magnetic

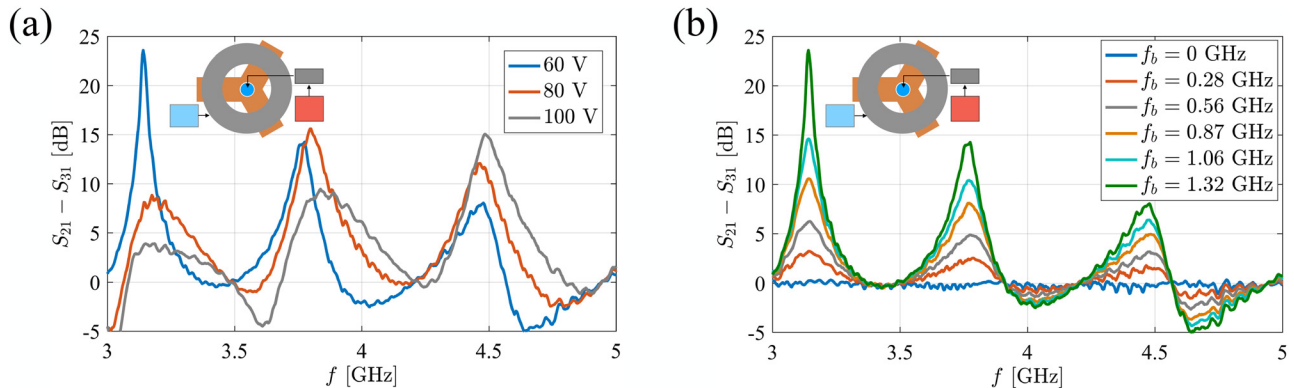


FIG. 12. Isolation measurements ($S_{21} - S_{31}$) for varying plasma frequencies and cyclotron frequencies. (a) The plasma's ionization is sustained by supplying 60, 80, and 100 V to the lamp's ballast that alters the plasma frequency ω_p , and the cyclotron frequency ω_b is kept fixed at 8.3×10^9 rad s^{-1} . (b) The cyclotron frequency $\omega_b = 2\pi f_b$ is swept from 0 to 8.3×10^9 rad s^{-1} as the plasma's ionization is sustained by supplying 60 V to the lamp's ballast.

fields ranging from 0 to 47 mT correspond to ω_b ranging from 0 to 8.3×10^9 rad s⁻¹, respectively. We note that some conventional ferrite-based circulators offer such tunability with electromagnets, although most employ permanent magnets. In our plasma case, we see that increasing the magnetic field increases the isolation at the three principal frequencies of interest. It is interesting to note that unlike plasma tuning, which broadens and slightly shifts the peaks with increased density, the increase in magnetic bias produces sharper features and greater isolation. While there may be an increased density with increased bias, due to better confinement of the plasma, it is more than compensated for by the increased isolation capacity. We note, however, that the strength of this isolation diminishes with increased field frequency as we move from one mode to another.

IV. DISCUSSION AND SUMMARY

The results presented here are qualitatively similar to those of Li *et al.*,³⁸ which were carried out with fields shaped by permanent magnets, resulting in much higher magnetic biasing of the plasma. Both show a significant tuning capability by varying plasma density, and a near linear dependence of the isolation on the strength of the magnetic bias. In all cases, broadening of the resonances arises due to electron collisional damping, and additional modes associated with return losses appear, due presumably to partial reflections from the plasma interface as the studies are carried out under conditions in which the plasma is overdense for the range of frequencies examined. The system is robust and provides isolation levels approaching 21 dB at 3.2 GHz, which constitutes a reasonable level, considering that typical levels achieved by commercial ferrite-based devices are in the 17–35 dB in the GHz range. Most commercial ferrite-based circulators also operate at much higher external magnetic biasing through the use of permanent magnets, typically in the 100 mT levels or higher depending on the magnetic permeability of the ferrite material. Here, the required bias to achieve reasonable isolation is in the 50 mT range.

A scaling to higher frequency will require preserving characteristic ratios, f_p/f and f_p/f_b , to achieve similar levels of isolation to those seen here. This will require significant increases in plasma density, which, for steady-state applications, may be challenging, but achieving the necessary conditions in pulsed discharge is potentially realizable. For example, operating in the 0.1–1 THz regime will require plasma diameters in the 0.5–0.05 mm range and plasma densities in the range of 10^{14} – 10^{16} cm⁻³. One promising approach to achieving such dense microplasma discharge columns is through ultra-short pulsed capillary discharges.^{39,40}

Finally, perhaps the most interesting attributes of the use of a plasma are its ability to absorb energy in high power applications. A plasma is self-healing, in which its absorption of energy leads to ionization and plasma heating and returns to its initial state via recombination. However, in absorbing energy, the plasma frequency changes, potentially detuning the device and compromising its isolation. In many practical applications, circulators are used to protect high power circuitry from back reflections. Clearly, more studies are required to better understand the performance of a plasma circulator under conditions where it presents a power-dependent (non-linear) response.

ACKNOWLEDGMENTS

This research was supported by an Air Force Office of Scientific Research Multi-University Research Initiative (MURI),

Grant No. FA9550–21-1-0244, with Dr. Mitat Birkan as program manager. L.H. acknowledges support of the Stanford France Center for Interdisciplinary Studies. We would also like to acknowledge the many regular inspiring discussions with our MURI, UCSD colleague D. Sievenpiper and researchers F. Li, R. Davis, and S. Kandil. Their recent paper³⁸ that describes similar studies was performed at higher magnetic biasing and with the use of permanent magnets, but, nevertheless, independently confirms the performance of these plasma circulators.

AUTHOR DECLARATIONS

Conflict of Interest

The authors have no conflicts to disclose.

Author Contributions

Hossein Mehrpour Bernety: Conceptualization (lead); Data curation (equal); Formal analysis (lead); Investigation (equal); Methodology (equal); Software (lead); Supervision (equal); Validation (equal); Visualization (equal); Writing – original draft (equal); Writing – review & editing (equal). **Luc Stephane Houriez:** Conceptualization (supporting); Data curation (lead); Formal analysis (lead); Investigation (equal); Methodology (equal); Supervision (equal); Validation (equal); Visualization (equal); Writing – original draft (equal); Writing – review & editing (equal). **Jesse Alexander Rodriguez:** Conceptualization (supporting); Data curation (supporting); Formal analysis (supporting); Investigation (supporting); Methodology (supporting); Supervision (supporting); Validation (supporting); Visualization (supporting); Writing – original draft (supporting); Writing – review & editing (supporting). **Benjamin Wang:** Conceptualization (supporting); Data curation (supporting); Formal analysis (supporting); Investigation (supporting); Methodology (supporting); Supervision (supporting); Validation (supporting); Visualization (supporting); Writing – original draft (supporting); Writing – review & editing (supporting). **Mark A. Cappelli:** Conceptualization (lead); Formal analysis (equal); Funding acquisition (lead); Methodology (supporting); Project administration (lead); Resources (lead); Supervision (lead); Writing – original draft (equal); Writing – review & editing (equal).

DATA AVAILABILITY

The data that support the findings of this study are available from the corresponding author upon reasonable request.

REFERENCES

- ¹D. M. Pozar, *Microwave Engineering* (John Wiley & Sons, 2011).
- ²E. F. Schloemann, “Circulators for microwave and millimeter-wave integrated circuits,” *Proc. IEEE* **76**, 188–200 (1988).
- ³L. Marzall, D. Psychogiou, and Z. Popović, “Microstrip ferrite circulator design with control of magnetization distribution,” *IEEE Trans. Microwave Theory Tech.* **69**, 1217–1226 (2021).
- ⁴C. H. Cox and E. I. Ackerman, “Review of radar system needs, and performance of techniques, for star,” in *IEEE Radar Conference (RadarConf22)* (IEEE, 2022), pp. 1–6.
- ⁵H. Ren, Y. Xie, H. Wei, P. Wu, and L. Dai, “A novel circulator construction with high multipactor threshold and high isolation for aerospace applications,” *IEEE Trans. Plasma Sci.* **50**, 715–720 (2022).

- ⁶Y. M. Jain, P. Sharma, K. Ambulkar, P. R. Parmar, A. R. Jadhav, and H. V. Dixit, "Steady-state operation of high CW power circulator: Challenges and solutions through simulation and experiments," *IEEE Trans. Plasma Sci.* **48**, 1290–1297 (2020).
- ⁷A. Fox, S. Miller, and M. Weiss, "Behavior and applications of ferrites in the microwave region," *Bell Syst. Tech. J.* **34**, 5–103 (1955).
- ⁸H. Bosma, "On stripline Y-circulation at UHF," *IEEE Trans. Microwave Theory Tech.* **12**, 61–72 (1964).
- ⁹U. Milano, J. Saunders, and L. Davis, "A Y-junction strip-line circulator," *IRE Trans. Microwave Theory Tech.* **8**, 346 (1957).
- ¹⁰C. Fay and R. Comstock, "Operation of the ferrite junction circulator," *IEEE Trans. Microwave Theory Tech.* **13**, 15–27 (1965).
- ¹¹H. Bosma, "On the principle of stripline circulation," *Proc. IEE-Part B* **109**, 137–146 (1962).
- ¹²D. C. Webb, "Design and fabrication of low-cost ferrite circulators," in *25th European Microwave Conference* (IEEE, 1995), Vol. 2, pp. 1191–1200.
- ¹³L. Martinez, V. Laur, A. L. Borja, P. Queffelec, and A. Belenguer, "Low loss ferrite Y-junction circulator based on empty substrate integrated coaxial line at Ku-band," *IEEE Access* **7**, 104789–104796 (2019).
- ¹⁴S. I. Shams, S. M. Sifat, M. Elsaadany, G. Gagnon, and A. A. Kishk, "Systematic design procedure for y-junction circulator based on ridge gap waveguide technology," *IEEE Trans. Microwave Theory Tech.* **69**, 2165–2177 (2021).
- ¹⁵T. Qiu, J. Wang, Y. Li, and S. Qu, "Circulator based on spoof surface plasmon polaritons," *IEEE Antennas Wireless Propag. Lett.* **16**, 821–824 (2016).
- ¹⁶M. Darques, J. De la Torre Medina, L. Piraux, L. Cagnon, and I. Huynen, "Microwave circulator based on ferromagnetic nanowires in an alumina template," *Nanotechnology* **21**, 145208 (2010).
- ¹⁷S. Barzanjeh, M. Wulf, M. Peruzzo, M. Kalae, P. Dieterle, O. Painter, and J. M. Fink, "Mechanical on-chip microwave circulator," *Nat. Commun.* **8**, 953 (2017).
- ¹⁸D. S. Sundar, C. Umamaheswari, T. Sridarshini, M. Karthikeyan, R. Sitharthan, A. S. Raja, and M. F. Carrasco, "Compact four-port circulator based on 2D photonic crystals with a 90° rotation of the light wave for photonic integrated circuits applications," *Laser Phys.* **29**, 066201 (2019).
- ¹⁹S. Tanaka, N. Shimomura, and K. Ohtake, "Active circulators-the realization of circulators using transistors," *Proc. IEEE* **53**, 260–267 (1965).
- ²⁰P.-H. Chen and R. M. Narayanan, "Design of active circulators using high-speed operational amplifiers," *IEEE Microwave Wireless Compon. Lett.* **20**, 575–577 (2010).
- ²¹G. Carchon and B. Nanwelaers, "Power and noise limitations of active circulators," *IEEE Trans. Microwave Theory Tech.* **48**, 316–319 (2000).
- ²²V. Dmitriev and W. Castro, "Dynamically controllable terahertz graphene Y-circulator," *IEEE Trans. Magn.* **55**, 18409700 (2018).
- ²³A. Kord, D. L. Sounas, and A. Alu, "Microwave nonreciprocity," *Proc. IEEE* **108**, 1728–1758 (2020).
- ²⁴G. D'Aguanno, D. L. Sounas, H. M. Saied, and A. Alù, "Nonlinearity-based circulator," *Appl. Phys. Lett.* **114**, 181102 (2019).
- ²⁵A. Mock, D. Sounas, and A. Alu, "Magnet-free circulator based on spatiotemporal modulation of photonic crystal defect cavities," *ACS Photonics* **6**, 2056–2066 (2019).
- ²⁶J. Wang, J. F. Herrmann, J. D. Witmer, A. H. Safavi-Naeini, and S. Fan, "Photonic modal circulator using temporal refractive-index modulation with spatial inversion symmetry," *Phys. Rev. Lett.* **126**, 193901 (2021).
- ²⁷R. O. Dendy, *Plasma Physics: An Introductory Course* (Cambridge University Press, 1995).
- ²⁸B. Wang, J. Rodríguez, and M. A. Cappelli, "3D woodpile structure tunable plasma photonic crystal," *Plasma Sources Sci. Technol.* **28**, 02LT01 (2019).
- ²⁹C. A. Balanis, *Advanced Engineering Electromagnetics* (John Wiley & Sons, 2012).
- ³⁰B. Wang and M. Cappelli, "A tunable microwave plasma photonic crystal filter," *Appl. Phys. Lett.* **107**, 171107 (2015).
- ³¹B. Wang and M. Cappelli, "A plasma photonic crystal bandgap device," *Appl. Phys. Lett.* **108**, 161101 (2016).
- ³²B. Wang and M. Cappelli, "Waveguiding and bending modes in a plasma photonic crystal bandgap device," *AIP Adv.* **6**, 065015 (2016).
- ³³G. Hagelaar and L. C. Pitchford, "Solving the Boltzmann equation to obtain electron transport coefficients and rate coefficients for fluid models," *Plasma Sources Sci. Technol.* **14**, 722 (2005).
- ³⁴L. S. Houriez, H. Mehrpour Bernety, J. A. Rodríguez, B. Wang, and M. A. Cappelli, "Experimental study of electromagnetic wave scattering from a gyro-tropic gaseous plasma column," *Appl. Phys. Lett.* **120**, 223101 (2022).
- ³⁵A. Latyshev and A. Yushmanov, "Interaction of electromagnetic E-wave with thin metal film," *Opt. Spectrosc.* **110**, 795–801 (2011).
- ³⁶S. Shinohara, Y. K. S. Shinohara, and Y. Kawai, "Skin depth of electromagnetic waves in plasma with magnetic field and collisions," *Jpn. J. Appl. Phys., Part 2* **35**, L725 (1996).
- ³⁷B. Wang, "A theoretical and experimental investigation of plasma photonic crystals and devices," Doctoral dissertation (Stanford University, 2022).
- ³⁸F. Li, R. J. Davis, S. M. Kandil, and D. F. Sievenpiper, "Electromagnetic nonreciprocity in a magnetized plasma circulator," [arXiv:2206.12507](https://arxiv.org/abs/2206.12507) (2022).
- ³⁹Y. Zhu, S. M. Starikovskaia, N. Y. Babaeva, and M. J. Kushner, "Scaling of pulsed nanosecond capillary plasmas at different specific energy deposition," *Plasma Sources Sci. Technol.* **29**, 125006 (2020).
- ⁴⁰A. Klochko, J. Lemainque, J.-P. Booth, and S. Starikovskaia, "Talif measurements of oxygen atom density in the afterglow of a capillary nanosecond discharge," *Plasma Sources Sci. Technol.* **24**, 025010 (2015).